Supplementary Material to the manuscript Sustainability-2585779

Pyrolysis and combustion characteristics of two Russian facemasks, kinetic modeling, gaseous emissions and pyrolysis by-products

Alexei Kangash, Damaris Kehrli, Pavel Maryandyshev, Alain Brillard, Valérie Tschamber

S1. Photos of the two face masks

Fig. S1 gathers photos of the two Russian face masks under consideration in the present study.



a) b)

Fig. S1. Photos of the Tissue a) and Surgical e) face masks commonly used in the Russian Federation.

S2. Operating conditions for the characterizations of the two masks

The proximate analyses of the masks were performed according to the ISO 1171 standards [17] and EN NF 18122 standards [18]. A Memmert VM400 oven was used to measure the moisture content (M). A sample was submitted to a temperature of 105 $\pm$ 2 °C during 24 hours. The fixed carbon (FC) and volatile matter (VM) contents were determined comparing the initial and final masses of the samples submitted to pyrolysis and combustion experiments in a thermobalance under the temperature ramp of 5 °C min^{-1}. The ash content of the masks was determined using a Nabertherm muffle furnace, according to NF EN ISO 18122, [18].

A calorimeter IKA C200 was used to determine the Higher Heating Value (HHV) of each mask.

An automatic elemental analyzer (EuroVector EA-3000) was finally used to perform the ultimate analyses of the masks, according to the ISO 29541, [19], ISO 19579, [20] and ASTM 3176-15, [21], standards.

Van Krevelen's formulas were applied to compute the atomic ratios H/C and O/C, [16]:

$$H/C = \frac{\frac{\%H}{1/NA}}{\frac{\%C}{12/NA}}; O/C = \frac{\frac{\%O}{16/NA}}{\frac{\%C}{12/NA}}, \qquad (S1)$$

where %H, %C and %O are the percentages of hydrogen, carbon and oxygen determined in the ultimate analysis and *NA* is the Avogadro number (*NA* = 6.02×10^{23} atoms per mol).

S3. Kinetic modeling through the Extended Independent Parallel Reaction model in the non-oxidative case (pyrolysis)

In the case of a non-oxidative atmosphere, the EIPR model consists in a set of ordinary differential equations, whose number is equal to the number of constituents to be taken into account, each equation describing the evolution of the mass of volatiles which are emitted from a constituent of the material. Each first-order ordinary differential equation is written as:

$$\frac{dm^e_{vol,i}}{dt}(t) = k_i\big(T(t)\big) f_i \left(m_i(0) - m^e_{vol,i}(t)\right), \qquad i = 1, \dots, I, \quad (S2)$$

where:

- $m^e_{vol,i}(t)$ is the mass of volatiles emitted from the constituent *i* of the sample (*i*=1,…,*I*).
- $k_i(T)$ is a kinetic constant which obeys an Arrhenius law: $k_i(T) = A_i \exp(-Ea_i/RT)$, where A_i (resp. Ea_i) is the pre-exponential factor (resp. the activation energy) for the constituent *i* and *R* is the ideal gas constant equal to 8.314 J mol^{-1} K^{-1}.
- $m_i(0)$ is the initial mass of the constituent *i*, which may be computed as a proportion of the overall mass of the sample: $m_i(0) = c_i\, m(0)$. This proportion c_i is considered as an unknown.
- f_i is a reaction function.
- $T(t)$ is the temperature (expressed in K) at time *t* in the sample. In the present experiments, the temperature $T(t)$ evolves with respect to the time parameter *t* with a constant rate: $T(t) = at + T_0$.

The initial value $m^e_{vol,i}(0) = 0$ is imposed.

Introducing the partial conversion $\alpha^e_{vol,i}(t) = m^e_{vol,i}(t)/m_i(0)$, Eq. (S2) can be rewritten as:

$$\frac{d\alpha^e_{vol,i}}{dt}(t) = k_i\big(T(t)\big)\frac{1}{m_i(0)} f_i\left(m_i(0)\left(1-\alpha^e_{vol,i}(t)\right)\right) = k_i\big(T(t)\big) f_i\left(\alpha^e_{vol,i}(t)\right), i = 1,\dots,I, \quad (S3)$$

up to a modification of the expression of the reaction function f_i. In most cases, a first-order reaction function, or Mampel's reaction function, with respect to the extent of conversion α, may be considered: $f_1(\alpha) = 1-\alpha$, whatever the constituent of each sample. In the present study, a fourth-order Avrami-Erofeev reaction function with respect to the extent of conversion α will also be considered for constituents of the two masks. It is defined as:

$$f_4(\alpha) = 4(1-\alpha)(-\log(1-\alpha))^{3/4}. \quad (S4)$$

Such an Avrami-Erofeev reaction function simulates in a better way the case of an intense devolatilization process, corresponding to a thin and high peak in the conversion rate curve.

To reduce the number of unknowns in the system (S3) (pre-exponential factor and activation energy for each kinetic constant, the relationships established in [*Brillard, A.; Brilhac, J.-F. Improved Relationships between Kinetic Parameters Associated with Biomass Pyrolysis or Combustion. Bioresource Technology* ***2021****, 342, 126053, doi:10.1016/j.biortech.2021.126053*] between pre-exponential factor and activation energy are used. They take the form:

$$A_{vol,i} = -\frac{Ea_{vol,i}T'(t_i^*)}{RT^2(t_i^*)} exp\left(\frac{Ea_i}{RT(t_i^*)}\right)\frac{1}{f_i'\left(\alpha(t_i^*)\right)}, \quad (S5)$$

where t_i^* is the time at which the maximal devolatilization occurs for the i-th constituent, $T(t_i^*)$ is the temperature at this time t_i^*, $\alpha(t_i^*)$ is the value of the global extent of conversion at this time t_i^*, and f_i' is the derivative of the reaction function f_i. The relationship (S5) only involves experimental data.

In the present study, the system of differential equations (S3) is solved using the Scilab software (version 6.0.2) and especially its routine 'ode', first with initial guesses of the kinetic parameters. The system (S3) is solved simultaneously for the four temperature ramps. The optimal values of the kinetic parameters are then determined using the routine 'datafit' of Scilab, that is minimizing with respect to these kinetic parameters the objective function chosen as the sum over the four temperature ramps of the expressions:

$$\sum_{i=1}^{I} c_i \sum_{j=1}^{J}\left(\left(\frac{d\alpha^e_{vol,i}}{dt}\right)_{exp}(t_j) - \left(\frac{d\alpha^e_{vol,i}}{dt}\right)_{sim}(t_j)\right)^2, \quad (S6)$$

where $\left(\frac{d\alpha^e_{vol,i}}{dt}\right)_{exp}(t_j)$ is the experimental conversion rate at time t_j and $\left(\frac{d\alpha^e_{vol,i}}{dt}\right)_{sim}(t_j)$ is the simulated conversion rate at time t_j, as deduced from the resolution of (S3), for each temperature ramp. For each temperature ramp, the total number *J* of time points t_j was taken equal to 400 to reduce the computation time, these time points t_j being regularly distributed along the overall duration of the thermogravimetric experiment.

Once the optimal values of the kinetic parameters are determined, the system (S3) is solved to obtain the simulated sample conversion and conversion rate as functions of time according to:

$$\alpha_{sim}(t) = \sum_{i=1}^{I} c_i \alpha_{vol,i}^{e}(t), \qquad (S7)$$

$$\frac{d\alpha_{sim}}{dt}(t) = \sum_{i=1}^{I} c_i \frac{d\alpha_{vol,i}^{e}(t)}{dt}, \qquad (S8)$$

for each temperature ramp. This allows comparing the experimental and simulated conversion and conversion rate curves of the material, and simultaneously for the four temperature ramps.

To validate the simulations, the maximal difference $max_j \left| \left(\frac{d\alpha_{vol,i}^{e}}{dt}\right)_{exp}(t_j) - \left(\frac{d\alpha_{vol,i}^{e}}{dt}\right)_{sim}(t_j) \right|$, hereafter denoted l_∞, and the square root $\left(\sum_{i=1}^{I} c_i \sum_{j=1}^{J} \left(\left(\frac{d\alpha_{vol,i}^{e}}{dt}\right)_{exp}(t_j) - \left(\frac{d\alpha_{vol,i}^{e}}{dt}\right)_{sim}(t_j) \right)^2 \right)^{1/2}$ of (S6), hereafter denoted l_2, between the experimental and simulated conversion rates are calculated for each temperature ramp. From these expressions, it is possible to deduce normalized expressions given in percentages. For each temperature ramp, R^2 determination coefficients are also calculated for the conversion according to the formula (no dimension):

$$R_m^2 = 1 - \frac{\sum_{j=1}^{J} \left(\alpha_{sim}(t_j) - \alpha_{exp}(t_j) \right)^2}{\sum_{j=1}^{J} \left(\alpha_{exp}(t_j) - \frac{1}{J} \sum_{k=1}^{J} \alpha_{exp}(t_k) \right)^2}, \qquad (S9)$$

where $\alpha_{sim}(t_j)$ and $\alpha_{exp}(t_j)$ are the simulated and experimental global conversions at time t_j, see (S7). Quite similar formulas may be built for the conversion rate (no dimension):

$$R_{mr}^2 = 1 - \frac{\sum_{j=1}^{N} \left(\left(\frac{d\alpha}{dt}\right)_{sim}(t_j) - \left(\frac{d\alpha}{dt}\right)_{exp}(t_j) \right)^2}{\sum_{j=1}^{N} \left(\left(\frac{d\alpha}{dt}\right)_{exp}(t_j) - \frac{1}{N} \sum_{k=1}^{N} \left(\frac{d\alpha}{dt}\right)_{exp}(t_k) \right)^2} \qquad (S10)$$

and for the overall variations (no dimension):

$$R_o^2 = 1 - \frac{\sum_{j=1}^{N} \left(\alpha_{sim}(t_j) - \alpha_{exp}(t_j) \right)^2}{\sum_{j=1}^{N} \left(\alpha_{exp}(t_j) - \frac{1}{N} \sum_{k=1}^{N} \alpha_{exp}(t_k) \right)^2} - \frac{\sum_{j=1}^{N} \left(\left(\frac{d\alpha}{dt}\right)_{sim}(t_j) - \left(\frac{d\alpha}{dt}\right)_{exp}(t_j) \right)^2}{\sum_{j=1}^{N} \left(\left(\frac{d\alpha}{dt}\right)_{exp}(t_j) - \frac{1}{N} \sum_{k=1}^{N} \left(\frac{d\alpha}{dt}\right)_{exp}(t_k) \right)^2}. \qquad (S11)$$

These determination coefficients should be as close to 1 as possible to validate the simulations.

S4. Kinetic modeling through the EIPR model in the case of an oxidative atmosphere (combustion)

Under an oxidative atmosphere, the devolatilization stages of the material surely occur. But the char structure is also degraded. The EIPR model considers that the constituents of the material lead to both the emission of volatiles and to the apparition of the char structure, once the volatiles are being emitted, this char structure being degraded at higher temperatures. The fraction of volatiles to be emitted from the constituent *i* is denoted as $\tau_{vol,i}$. The complement of $\tau_{vol,i}$ to 1 represents the fraction of char which appears from the constituent *i* during the devolatilization stage and which will be degraded during the further combustion stage.

Under an oxidative atmosphere, the EIPR model first simulates the evolution of the mass of volatiles which are emitted from the constituent *i* of the material with respect to time according to the first-order ordinary differential equation:

$$\frac{dm_{vol,i}^{e}}{dt}(t) = k_i\big(T(t)\big) f_i\left(m_i(0)\tau_{vol,i} - m_{vol,i}^{e}(t)\right), i = 1, \dots, I, \quad (S13)$$

where:

- $m_{vol,i}^{e}(t)$ is the mass of volatiles emitted by the constituent *i* of the sample (*i*=1,…,*I*).
- k_i is a kinetic constant which obeys an Arrhenius law: $k_i(T) = A_i \exp(-Ea_i/RT)$, where A_i (resp. Ea_i) is the pre-exponential factor (resp. the activation energy) for the devolatilization of the constituent *i*.
- $m_i(0)$ is the initial mass of the constituent *i*, which may be computed as a proportion of the overall mass of the sample: $m_i(0) = c_i\, m(0)$. This proportion c_i is considered as an unknown.
- $T(t)$ is the temperature at time *t* in the sample (expressed in K) and which evolves with respect to the time parameter *t* with a constant rate: $T(t) = at + T_0$.
- f_i is a reaction function.
- $\tau_{vol,i}$ is the fraction of volatiles contained in the constituent *i* and which will be emitted during the devolatilization stage, as previously exposed. This fraction $\tau_{vol,i}$ is considered as an unknown.

The presence of the fraction $\tau_{vol,i}$ of volatiles emitted by the constituent *i* of the sample is the unique difference between the equations (S3) and (S10).

The initial value $m_{vol,i}^{e}(0) = 0$ is imposed.

The evolution with respect to time of the mass $m_{char,i}^{c}$ of char which appears during the devolatilization of the constituent *i* and which is consumed is described according to the first-order ordinary differential equation:

$$\frac{dm_{char,i}^{c}}{dt}(t) = k_{comb}\big(T(t)\big)\left(\frac{1-\tau_{vol,i}}{\tau_{vol,i}} m_{vol,i}^{e}(t) - m_{char,i}^{c}(t)\right) P_{O_2}, \quad (S14)$$

where the kinetic constant $k_{comb}(T)$ obeys an Arrhenius law: $k_{comb}(T) = A_{comb} exp(-Ea_{comb}/RT)$ and where P_{O_2} is the oxygen pressure which is constant during the experiment ($P_{O_2} = 2.1 \times 10^4$ Pa). The initial value $m_{char,i}^{c}(0) = 0$ is imposed, as no char is being consumed at the beginning of the combustion process. The kinetic constant k_{comb} is the same for the combustion of the chars produced from all constituents of each mask. A first-order reaction function is usually sufficient to simulate the char combustion.

Introducing the partial conversions:

$$\alpha_{vol,i}^{e}(t) = \frac{m_{vol,i}^{e}(t)}{m_i(0)\tau_{vol,i}};\ \alpha_{char,i}^{c}(t) = \frac{m_{char,i}^{c}(t)}{m_i(0)\big(1-\tau_{vol,i}\big)}, \quad (S15)$$

The equations (S13)-(S14) become:

$$\frac{d\alpha_{vol,i}^{e}}{dt}(t) = k_i\big(T(t)\big)\frac{1}{m_i(0)\tau_{vol,i}} f_i\left(m_i(0)\tau_{vol,i}\left(1-\alpha_{vol,i}^{e}(t)\right)\right) = k_i\big(T(t)\big) f_i\left(\alpha_{vol,i}^{e}(t)\right), i = 1, \dots, I, \quad (S16)$$

$$\frac{d\alpha_{char,i}^{c}}{dt}(t) = k_{comb}\big(T(t)\big)\left(\alpha_{vol,i}^{e}(t) - \alpha_{char,i}^{c}(t)\right) P_{O_2}, i = 1, \dots, I. \quad (S17)$$

The system (S16)-(S17) is solved with a procedure adapted from that described in the preceding section 3 for the pyrolysis case. The relationships between pre-exponential factor and activation energy presented in (S5) and accounting for the devolatilization stage will also be used in this combustion case, together to a quite similar relationship established in *[Brillard, A.; Brilhac, J.-F. Improved Relationships between Kinetic Parameters Associated with Biomass Pyrolysis or Combustion. Bioresource Technology **2021**, 342, 126053, doi:10.1016/j.biortech.2021.126053*] in the case of the char combustion.

S5. Experimental conditions for the gas chromatography analyses

The diameter of the capillary column is equal to 0.25 mm. The fixed phase thickness is equal to 0.25 µm. The column length is equal to 30 m. A sample was introduced with a split ratio 1:100. The input temperature was chosen equal to 280 °C. Helium was taken as carrier gas. A constant pressure gas

flow was controlled and the flow through the column was fixed at 1.2 mL min^{-1}. The temperature was increased to and maintained constant at 40 °C for 5 min, then increased with a rate of 20 °C min^{-1} to 280 °C, and finally increased with a rate of 15 °C min^{-1} to the final temperature equal to 300, 400 or 500 °C and kept constant for 5 min. The temperature of the transfer line with the mass detector was held at 280 °C and the temperature of the ion source was held at 230 °C. The ionization energy was 70 eV. The detector voltage was 1.07 kV (according to the automatic configuration), and the mass detector worked in the mass spectra scanning mode (TIC Scan) in the mass range 15–600 Da.

S6. Experimental conditions for the combustion experiments performed in the horizontal oven

The alumina reactor placed in the Nabertherm oven has a length equal to 1 m and a diameter equal to 57 mm. A mask sample (between 0.2 and 0.5 g) was placed in an alumina boat and manually introduced at room temperature into the isothermal zone of the reactor. An air flow was then injected with a flow rate of 100 Nl h^{-1}. The temperature was increased from room temperature to 900 °C with a temperature ramp approximately equal to 5 °C min^{-1}.

The gaseous emissions were continuously measured at the outlet of the reactor using a multi-component NGA2000 Rosemount analyzer, with a flame-ionization detector or an infrared cell (for the NO emissions). Such a gaseous analyzer usually detects chemical compounds only with a number of carbon atoms lower than 10.

S7. Further characterizations concerning the pyrolysis and combustion experiments

Table S1 gathers details concerning the conversion and conversion rate curves for each mask when submitted to pyrolysis, together with the final sample mass, for each temperature ramp. The conversion range represents the temperature interval during which the conversion lies between 0.05 and 0.95.

Table S1. Conversion range. Position and height of the unique devolatilization peak, for the two masks and the four pyrolysis cases. Final sample mass in each case. Comparison with results of the literature.

Sample	Conversion range	Devolatilization peak		Final sample mass
	(°C)	Temperature (°C)	Maximal conversion rate (1/s)	(%)
Tissue				
R5	304.7-845.3	358.2	0.199	7.5
R10	314.5-834.1	371.0	0.377	6.8
R15	321.2-833.3	377.6	0.553	6.6
R20	327.1-819.6	381.8	0.743	6.5
Surgical				
R5	391.1-466.9	448.0	0.203	5.1
R10	410.1-479.2	459.5	0.435	5.1
R15	413.2-489.0	467.6	0.638	4.3
R20	426.1-495.0	472.7	0.913	4.5
Cotton fabric [Br1]				
R5	296.1-834.1	332.5	0.183	10.0
R10	306.5-799.7	342.7	0.342	13.3
R20	318.3-707.7	357.7	0.641	13.3
Tissue mask ECLT [Br2]				

R5	286.4-572.1	349.9	0.206	11.7
R10	298.5-618.8	363.1	0.377	11.1
R15	304.9-531.0	369.3	0.558	11.6
R20	307.7-599.8	373.1	0.699	10.5
Polypropylene terephthalate [Dha]				
R5	350-480	420	0.183	
R10	360-500	435	0.350	
R20	380-520	450	0.633	
Polypropylene	337-471			
Korean surgical mask (whole mask, R10) [Jun]	330-495	455		
SGP2 face mask [Br2]				
R5	410.2-688.0	447.5	0.247	4.0
R10	412.6-480.9	460.3	0.445	4.1
R15	427.9-482.6	467.2	0.708	3.6
R20	437.6-489.6	471.5	0.929	4.2

[Br1] Brillard, A.; Habermacher, D.; Brilhac, J.-F. Thermal Degradations of Used Cotton Fabrics and of Cellulose: Kinetic and Heat Transfer Modeling. *Cellulose* **2017**, *24*, 1579–1595, doi:10.1007/s10570-017-1200-6.

[Br2] Brillard, A.; Kehrli, D.; Douguet, O.; Gautier, K.; Tschamber, V.; Bueno, M.-A.; Brilhac, J.-F. Pyrolysis and Combustion of Community Masks: Thermogravimetric Analyses, Characterizations, Gaseous Emissions, and Kinetic Modeling. *Fuel* **2021**, *306*, 121644, doi:10.1016/j.fuel.2021.121644.

[Dh] Dhahak, A.; Hild, G.; Rouaud, M.; Mauviel, G.; Burkle-Vitzthum, V. Slow Pyrolysis of Polyethylene Terephthalate: Online Monitoring of Gas Production and Quantitative Analysis of Waxy Products. *Journal of Analytical and Applied Pyrolysis* **2019**, *142*, 104664, doi:10.1016/j.jaap.2019.104664.

[Jun] Jung, S.; Lee, S.; Dou, X.; Kwon, E.E. Valorization of Disposable COVID-19 Mask through the Thermo-Chemical Process. *Chemical Engineering Journal* **2021**, *405*, 126658, doi:10.1016/j.cej.2020.126658.

Table S2 gives the positions and heights of the peaks and the final masses for the combustion of the two masks, under the different temperature ramps.

Table S2. Conversion range. Position and height of each peak and final sample mass, for the two masks and the four combustion cases.

Sample	Conversion range	First peak		Second peak		Final mass
	(°C)	Temperature (°C)	Maximal conversion rate (1/s)	Temperature (°C)	Maximal conversion rate (1/s)	(%)
Tissue						
R5	291.7-476.2	332.8	0.329	454.5	0.022	1.5
R10	305.5-493.1	348.6	0.644	468.8	0.034	2.2
R15	307.8-502.4	357.9	0.901	478.5	0.053	1.7
R20	309.3-514.1	366.5	1.116	488.4	0.067	1.6
Surgical						
R5	232.6-380.5	256.6	0.209	-	-	6.5
R10	237.0-415.8	274.7	0.269	-	-	3.7
R15	252.0-418.5	302.6	0.460	-	-	4.5
R20	257.2-446.4	318.1	0.558	-	-	4.3
Cotton fabrics [Br1]						
R5	284.0-460.3	312.9	0.231	447.4	0.032	0.1
R10	297.0-594.7	326.1	0.469	459.2	0.065	2.0
R20	340.0-465.0	340.1	0.984	458.9	0.207	1.9
Tissue ECLT [Br2]						

R5	256.8-458.1	331.4	0.099	431.9	0.053	1.4
R10	267.2-475.0	341.9	0.198	438.3	0.305	1.2
R15	273.3-488.7	344.5	0.306	435.3	0.252	1.0
R20	277.3-487.3	343.2	0.470	433.7	0.254	1.2
Surgical SGP2						
[Br2]						
R5	248.4-356.6	246.6	0.165	-	-	2.8
R10	246.6-444.5	283.3	0.337	-	-	3.2
R15	258.1-483.7	302.0	0.467	-	-	1.5
R20	259.5-577.3	301.6	0.399	-	-	3.9
Polypropylene	280-350					
R10 [29]						

[Br1] Brillard, A.; Habermacher, D.; Brilhac, J.-F. Thermal Degradations of Used Cotton Fabrics and of Cellulose: Kinetic and Heat Transfer Modeling. *Cellulose* **2017**, *24*, 1579–1595, doi:10.1007/s10570-017-1200-6.

[Br2] Brillard, A.; Kehrli, D.; Douguet, O.; Gautier, K.; Tschamber, V.; Bueno, M.-A.; Brilhac, J.-F. Pyrolysis and Combustion of Community Masks: Thermogravimetric Analyses, Characterizations, Gaseous Emissions, and Kinetic Modeling. *Fuel* **2021**, *306*, 121644, doi:10.1016/j.fuel.2021.121644.

In [14], the authors performed combustion experiments on Surgical masks built with polypropylene and polyester under a temperature ramp of 10 °C/min. They found a main peak at 305 °C and a very much smaller peak at 475 °C.

S8. Comparison between the pyrolysis and combustion profiles of the two masks

Comparing the thermogravimetric profiles of the two face masks under the temperature ramp of 5 °C/min leads to the curves gathered in Fig. S2.

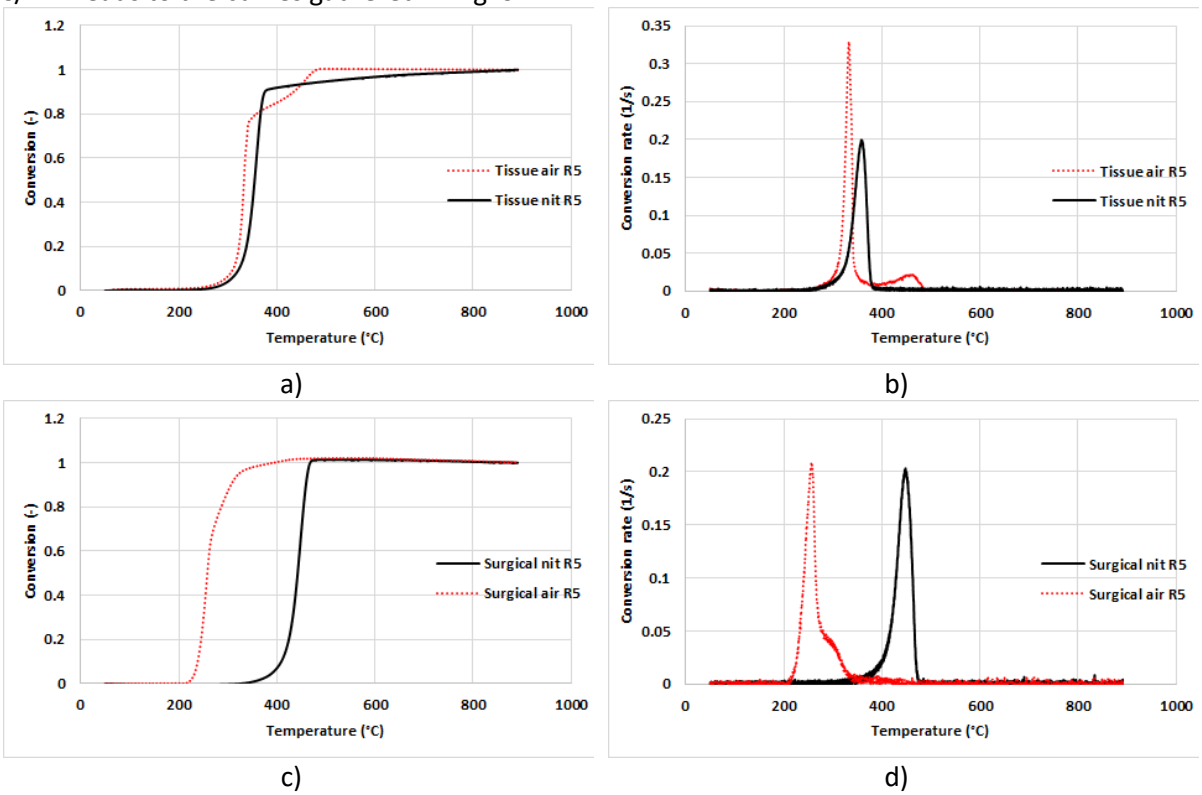


Fig. S2. Conversion and conversion rate curves for the Tissue mask a) and b), and for the Surgical mask c) and d).

For both masks, the conversion curves start earlier under air than under nitrogen and the unique peak of the combustion curves is shifted to lower temperatures. This shift is especially important for the Surgical mask: +176.8 °C, to be compared to +25.4 °C for the Tissue mask. For the Tissue mask, the combustion peak is thinner and higher under air than under nitrogen. Oxygen is known to enhance the reaction. A second peak appears on the combustion profile of the Tissue mask under air, which is much lower than the first one. It certainly corresponds to the combustion of the remaining char structure of the fibers. This explains the significant change of shape between the conversion curves for the Tissue mask under nitrogen and under air. For the Surgical mask, a shoulder appears on the right-hand side of the unique combustion peak.
Similar observations can be brought for the other temperature ramps.

S9. Chromatogram peaks for the two masks

Table S3. Chromatogram peaks for the two masks under the isothermal temperatures of 300, 400 and 500 °C.

Species	Temperature (°C)			Species	Temperature (°C)		
Textile				Surgical			
	500	400	300		500	400	300
(2H) - furan - 2 - one	8480	10055		(2,2,6,6-TETRAMETHYLCYCLOHEXYL)METHANOL	3068	344	
.alpha.-D-Glucopyranose, 4-O-.beta.-D-galactopyranosyl-	652	445		(2,4,6-Trimethylcyclohexyl) methanol	18084	40	
.beta.-D-Glucopyranose, 1,6-anhydro-		19637		(3E)-2,3,5-TRIMETHYL-1,3-HEXADIENE	2848		
.beta.-D-Glucopyranose, 1,6-anhydro-		1120		1,1'-Bicyclohexyl, 2-(1-methylethyl)-, trans-	1543		
1-(acetyloxy)-2-propanone	6969			1,5-Hexadiene, 2,5-dimethyl- (CAS)	4239		
1-Hexanol, 2-ethyl-			27	10-Dodecen-1-ol, 7,11-dimethyl-	4671		
1,2,3-Benzenetriol	4946	7329		10-Methylnonadecane		38	
1,2-Butanediol, 3,3-dimethyl-		920		11-Methyldodecanol	16017	1939	
1,2-Cyclopentanedione	11296	8500		18-Nonadecen-1-ol	711		
1,3-Benzenediol, 5-methyl-		909		1-BUTYL-2-PROPYLCYCLOPENTANE	666		
1,3-DIPHENYL-1,3,5,5-TETRAMETHYL CYCLOTRISILOXANE	81336			1-Cyclopentyleicosane		52	
1,3-Dihydroxyacetone dimer		8930		1-Decanol, 2-hexyl-	16340		24
1,3-Dioxol-2-one,4,5-dimethyl-		3049		1-Decene, 4-methyl-	857		
1,4:3,6-Dianhydro-.alpha.-d-glucopyranose	2954	5464		1-Dodecanol, 2-hexyl-		634	
1,4-Dioxan-2-ol	133			1-Dodecanol, 2-octyl-	16340	1234	
1,6-Anhydro-.beta.-D-glucofuranose	6212	9698		1-Dodecanol, 3,7,11-trimethyl-	1818		
1,6-ANHYDRO-BETA-D-GLUCOPYRANOSE		1844		1-ETHYL-2-PROPYLCYCLOHEXANE	5302		
1-Dodecanol		332		1-Heptadecanol (CAS)		39	
2(3H)-Furanone	2367			1-Heptanol, 2,4-diethyl-	6652		
2(5H)-Furanone	5960	5143		1-Heptene, 2,6-dimethyl-	1244		
2,3-Anhydro-d-mannosan	751	956		1-Heptene, 2-methyl-	1093		
2,3-Pentadienoic acid-, ethyl ester		280		1-Hexadecanol, 3,7,11,15-tetramethyl-	10820		
2,5-Furandione, dihydro-3-methyl-	965	1309		1-Hexene, 2,5-dimethyl- (CAS)	1400		
2,5-Furandione, dihydro-3-methyl-		1384		1-Hexene, 3,3,5-trimethyl-	9717		

2-Butenal, 2-methyl-, (E)-	5676		
2-Butenoic acid, methyl ester, (Z)-	950		
2-Cyclohexen-1-ol	2001	1255	
2-Cyclopenten-1-one, 2-hydroxy-3-methyl-	3775	2966	
2-Cyclopenten-1-one, 2-methyl-	567		
2-furan-carboxaldehyde	11270	15273	
2-Furancarboxaldehyde, 5-methyl-		2570	
2-FURANCARBOXALDEHYDE, 5-(HYDROXYMETHYL)-	23200		
2-Furanmethanol	2741	2814	
2H-Pyran-2-methanol, tetrahydro-			49
2H-Pyran-2,6(3H)-dione		1251	
2-Hydroxy-2-cyclopenten-1-one			50
2-Hydroxy-gamma-butyrolactone		1658	
2-Propenoic acid, 2-methyl-, oxiranylmethyl ester		856	
2-oxo-propanoic acid, methyl ester	29627		
3-Furaldehyde	1347	837	
3-Hydroxy-4-pyrone	2876	2489	
3-METHYLENEDIHYDRO-2,5-FURANDIONE	962	1058	
4-Cyclopentene-1,3-dione	533		
4H-Pyran-4-one, 2,3-dihydro-3,5-dihydroxy-6-methyl-	2674	2340	81
4-Methyl-2-oxo-(1H)-pyrimidine		1228	
4-Methyl-2-oxopentanenitrile	8594	9008	
4-Methyl-5H-furan-2-one	1624	1428	
5-Hydroxymethylfurfural		35688	107
5 METHYL FURFURAL	1877		
5,9-Dodecadien-2-one, 6,10-dimethyl-, (E,E))-	3947		
Acetic acid, 2-ethylhexyl ester	1350		
Acetic acid, methyl ester	13832	12173	
anhydro - sugar	3641	4971	206
Bis(2-ethylhexyl) maleate			32
Butanedial	5714		
1-Methyl-2-methylenecyclohexane	2321		
1-METHYL-3-(2-METHYL-2-PROPENYL)CYCLOPENTANE	446		
1-Nonene, 4,6,8-trimethyl-	662		
1-Octene, 3-ethyl-	608		
1-Octene, 3,7-dimethyl-		195	
1-tridecanol			10
1-Tridecene	1324		
1-Undecene		1231	
1-Undecene, 8-methyl-	19592		
2,3-Dimethyl-3-heptene			
2,4-Dimethyl-1-heptene	31534	4251	
2,6-Octadiene, 2,4-dimethyl-	1720		
2-Decene, 4-methyl-, (Z)-		64	
2-Isopropyl-5-methyl-1-heptanol	13011	103	
2-Methylbicyclo[3.2.1]octane	952		
2-methylhexacosane	579		
2-Octene, 3,7-dimethyl-, (Z)-	712		
2-Undecene, 4,5-dimethyl-, [R*,R*-(E)]-	2572		
3-Octene, 4-ethyl-	391		
3-Tetradecyne (CAS)	193		
4-Hepten-3-ol, 4-methyl-	350		
4-Methyl-1,5-heptadiene	2094		
4-Methyl-2-heptene	13228		
5,7-DIMETHYL-6-OCTEN-1-OL	1870		
6-Octen-1-ol, 3,7-dimethyl-	1270		
Bicyclo[3.1.1]heptane, 2,6,6-trimethyl-	167		
cis-3-Hexenyl heptine carbonate	11211		
Cyclohexane, (1,2-dimethylbutyl)-	2219		
Cyclohexane, 1,2,3,5-tetraisopropyl-	27191		
Cyclohexane, 1,3,5-trimethyl-	14795	236	
Cyclohexane, 1-ethyl-2-propyl-	7228		

But-1-ene-3-yne, 1-ethoxy-		4354
Carbamic acid, (3,4,4-trimethyl-1,2-dioxetan-3-yl)methyl ester		6419
Cyclohexene, 1-methyl-4-(1-methylethenyl)-	476	
D-Allose	290364	
Dihydroxyacetone	5519	
Diisooctyl maleate		70
Ethanone, 1-(2-furanyl)-	896	219
Hexadecane	195	
HYDROXY DIMETHYL FURANONE	2367	4332
m-Cresol	829	
METHYL 2-OXOPROPANOATE		24850
Oxirane, [(tetradecyloxy)methyl]-	733	
Propanal		3374
Propanoic acid, ethenyl ester	1455	
Styrene	3365	
VINYL (2E)-2-BUTENOATE	1460	
Vinyl crotonate		1459

Cyclohexane, 2,4-diethyl-1-methyl-	2532		
Cyclohexene, 3-(2-methylpropyl)-	257		
Cyclooctanemethanol	6692		
Cyclopentane, 1,2-dimethyl-3-(1-methylethyl)-	1070		
Cyclopentane, 1-pentyl-2-propyl-			7
Cyclopentanone, 2-methyl-		35	
Cyclopentene, 1,2,3-trimethyl-	4487		
Cyclopropane, 1,1-dimethyl-2-(2-methyl-1-propenyl)-	3799		
Diisodecyl ether			20
Docosane		82	73
Dodecane, 2,6,11-trimethyl-	1053	46	
Dodecane, 4,6-dimethyl-	1106	52	
Dotriacontane		356	
Eicosane			18
Heptane, 2,5,5-trimethyl- (CAS)		87	
Heptane, 3,3,5-trimethyl- (CAS)	4747		
Heptane, 4-methyl-	16499	288	
Hexadecane		253	55
Hexadecane, 2,6,11,15-tetramethyl-			14
Hexane, 2,4-dimethyl-	2370		
hydroxymethylcyclododecane	12193		
Isotridecanol-	19253	2347	16
Methyl tetrahydroionol	215		
Nonadecane, 2-methyl- (CAS)			23
Nonane, 5-methyl-5-propyl-	307		
Nonahexacontanoic acid			31
Octadecane		714	
Octane, 2,3-dimethyl-	210		
OCTANE, 3,3-DIMETHYL-		325	
Octane, 4,5-diethyl-	567		

Octadecanoic acid		19
Oxalic acid, 6-ethyloct-3-yl hexyl ester		13
Oxalic acid, bis(6-ethyloct-3-yl) ester		12
Pentylidenecyclohexane	431	
Tridecanol	22343	7

Table S4. Main chromatogram peaks for the two masks under the highest isothermal temperature of 500 °C (peak area greater than 1000).

Textile		Surgical	
Species	500 °C	Species	500 °C
D-Allose	290364	2,4-Dimethyl-1-heptene	31534
1,3-DIPHENYL-1,3,5,5-TETRAMETHYL CYCLOTRISILOXANE	81336	Cyclohexane, 1,2,3,5-tetraisopropyl-	27191
2-oxo-propanoic acid, methyl ester	29627	Tridecanol	22343
2-FURANCARBOXALDEHYDE, 5-(HYDROXYMETHYL)-	23200	1-Undecene, 8-methyl-	19592
Acetic acid, methyl ester	13832	Isotridecanol-	19253
1,2-Cyclopentanedione	11296	(2,4,6-Trimethylcyclohexyl) methanol	18084
2-furan-carboxaldehyde	11270	Heptane, 4-methyl-	16499
4-Methyl-2-oxopentanenitrile	8594	1-Decanol, 2-hexyl-	16340
(2H) - furan - 2 - one	8480	1-Dodecanol, 2-octyl-	16340
1-(acetyloxy)-2-propanone	6969	11-Methyldodecanol	16017
1,6-Anhydro-.beta.-D-glucofuranose	6212	Cyclohexane, 1,3,5-trimethyl-	14795
2(5H)-Furanone	5960	4-Methyl-2-heptene	13228
Butanedial	5714	2-Isopropyl-5-methyl-1-heptanol	13011
2-Butenal, 2-methyl-, (E)-	5676	hydroxymethylcyclododecane	12193
Dihydroxyacetone	5519	cis-3-Hexenyl heptine carbonate	11211
1,2,3-Benzenetriol	4946	1-Hexadecanol, 3,7,11,15-tetramethyl-	10820
5,9-Dodecadien-2-one, 6,10-dimethyl-, (E,E))-	3947	1-Hexene, 3,3,5-trimethyl-	9717
2-Cyclopenten-1-one, 2-hydroxy-3-methyl-	3775	Cyclohexane, 1-ethyl-2-propyl-	7228
anhydro - sugar	3641	Cyclooctanemethanol	6692
Styrene	3365	1-Heptanol, 2,4-diethyl-	6652
1,4:3,6-Dianhydro-.alpha.-d-glucopyranose	2954	1-ETHYL-2-PROPYLCYCLOHEXANE	5302
3-Hydroxy-4-pyrone	2876	Heptane, 3,3,5-trimethyl- (CAS)	4747
2-Furanmethanol	2741	10-Dodecen-1-ol, 7,11-dimethyl-	4671
4H-Pyran-4-one, 2,3-dihydro-3,5-dihydroxy-6-methyl-	2674	Cyclopentene, 1,2,3-trimethyl-	4487
2(3H)-Furanone	2367	1,5-Hexadiene, 2,5-dimethyl- (CAS)	4239
HYDROXY DIMETHYL FURANONE	2367	Cyclopropane, 1,1-dimethyl-2-(2-methyl-1-propenyl)-	3799
2-Cyclohexen-1-ol	2001	(2,2,6,6-TETRAMETHYLCYCLOHEXYL)METHANOL	3068
5 METHYL FURFURAL	1877	(3E)-2,3,5-TRIMETHYL-1,3-HEXADIENE	2848

4-Methyl-5H-furan-2-one	1624
VINYL (2E)-2-BUTENOATE	1460
Propanoic acid, ethenyl ester	1455
Acetic acid, 2-ethylhexyl ester	1350
3-Furaldehyde	1347

2-Undecene, 4,5-dimethyl-, [R*,R*-(E)]-	2572
Cyclohexane, 2,4-diethyl-1-methyl-	2532
Hexane, 2,4-dimethyl-	2370
1-Methyl-2-methylenecyclohexane	2321
Cyclohexane, (1,2-dimethylbutyl)-	2219
4-Methyl-1,5-heptadiene	2094
5,7-DIMETHYL-6-OCTEN-1-OL	1870
1-Dodecanol, 3,7,11-trimethyl-	1818
2,6-Octadiene, 2,4-dimethyl-	1720
1,1'-Bicyclohexyl, 2-(1-methylethyl)-, trans-	1543
1-Hexene, 2,5-dimethyl- (CAS)	1400
1-Tridecene	1324
6-Octen-1-ol, 3,7-dimethyl-	1270
1-Heptene, 2,6-dimethyl-	1244
Dodecane, 4,6-dimethyl-	1106
1-Heptene, 2-methyl-	1093
Cyclopentane, 1,2-dimethyl-3-(1-methylethyl)-	1070
Dodecane, 2,6,11-trimethyl-	1053

S10. Further characteristics of the main gaseous emissions occurring during combustion experiments performed on the two masks

Table S5 presents further characteristics of the overall gaseous emissions presented in Fig. 5.

Table S5. Positions and heights of the peaks of the main gaseous emissions.

Sample	Peak CO		Peak CO_2		Peak THC	
	Position (°C)	Height (ppm/g)	Position (°C)	Height (ppm/g)	Position (°C)	Height (ppm/g)
Tissue	344.4	9127	343.6	15607	340.5	8164
	452.2	11248	448.7	19937	-	-
Surgical	376.6	9731	376.2	3157	377.7	34148

For the CO emissions, the peak of the Surgical mask lies between the two peaks of the Tissue mask. It is larger than the thin needles of the two peaks observed for the Tissue mask. Its height also lies between the heights of the two peaks of the Tissue mask. For the CO_2 emissions, the peak of the Surgical mask lies between the two peaks of the Tissue mask. Its height is much smaller than that of the two peaks of the Tissue mask. For the THC emissions, the peak of the Surgical mask appears at a higher temperature than that of the Tissue mask. Its height is much higher than that of the Tissue mask.

Integrating the area below each emission curve presented in Fig. 5 returns the overall amount of gas emitted, for each gas considered in the present study. Figure S3 presents these overall amounts converted in moles per gram of material.

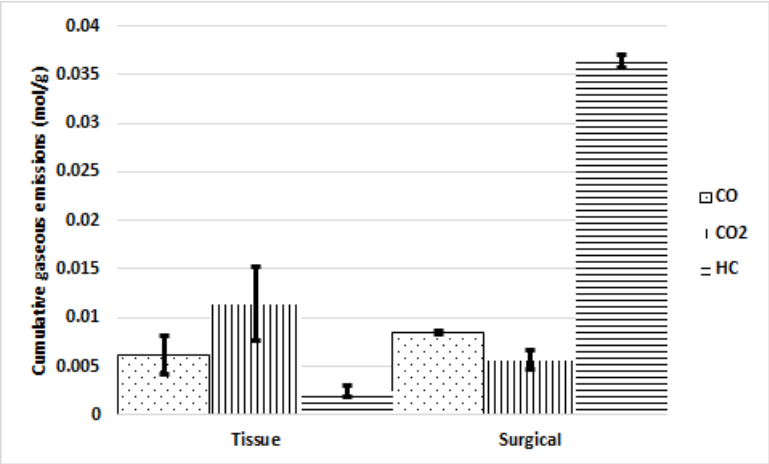


Fig. S3. Overall gaseous amounts (CO dotted, CO_2 vertical lines, and total hydrocarbons (HC) horizontal lines).

The overall CO amounts are quite equal for the two masks: 7.7×10^{-3} mol/g, for the Tissue mask and 1.2×10^{-2} mol/g, for the Surgical mask. The overall CO_2 amounts are higher for the Tissue mask than for the Surgical one. The overall THC amounts are much lower for the Tissue mask than for the Surgical one (approximately three times lower), because the C fraction of the Surgical mask is much higher. CO_2 emissions are the highest emissions tor the Tissue mask, while THC emissions are the highest emissions for the Surgical mask. These differences between the two masks may be explained by the fibers they are built with.

During the combustion of polypropylene fibers, the CO emissions were observed to present a unique peak occurring between 60 and 170 °C, [*Le Bras, M.; Duquesne, S.; Fois, M.; Grisel, M.; Poutch, F. Intumescent Polypropylene/Flax Blends: A Preliminary Study. Polymer Degradation and Stability 2005, 88, 80–84, doi:10.1016/j.polymdegradstab.2004.04.028*]. In [*Jung, S.; Lee, S.; Dou, X.; Kwon, E.E. Valorization of Disposable COVID-19 Mask through the Thermo-Chemical Process. Chemical*

Engineering Journal 2021, 405, 126658, doi:10.1016/j.cej.2020.126658], the authors measured the gaseous emissions (mainly THC) occurring during the pyrolysis of a Korean surgical mask. A unique peak was observed in the temperature range 495-505 °C for CH_4, C_2H_6 and C_2H_4. In [*Dhahak, A.; Hild, G.; Rouaud, M.; Mauviel, G.; Burkle-Vitzthum, V. Slow Pyrolysis of Polyethylene Terephthalate: Online Monitoring of Gas Production and Quantitative Analysis of Waxy Products. Journal of Analytical and Applied Pyrolysis 2019, 142, 104664, doi:10.1016/j.jaap.2019.104664*], the authors observed a maximal CO emission at 444 °C, when performing the slow pyrolysis of pure polyethylene terephthalate. This position of the maximal value is comparable to the position (376.6 °C) of the CO emissions in the case of the Surgical mask.

S11. Comparisons between the conversion rate curves associated to the combustion and the gaseous emissions

Figure S4 superimposes the conversion rate curves and the gaseous emissions continuously measured during combustion processes performed (in the thermobalance and in the horizontal oven) under the temperature ramp of 5 °C/min.

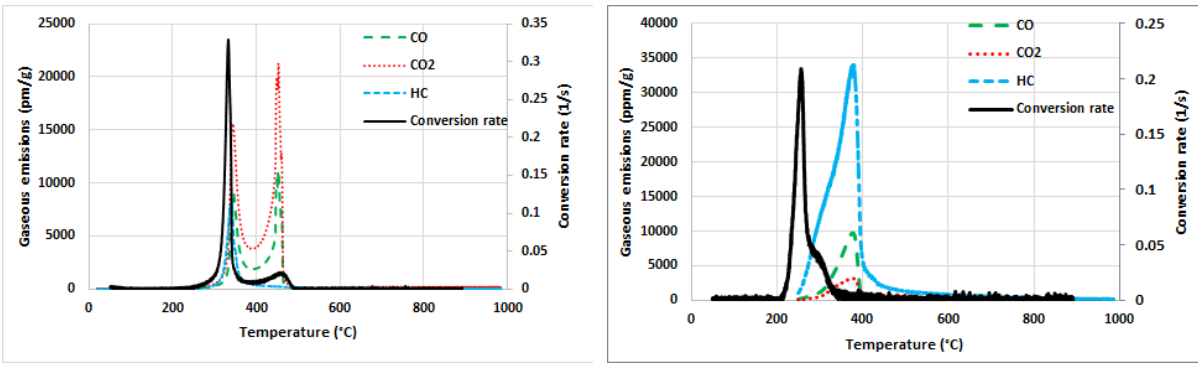


Fig. S4. Conversion rate curves of the combustion processes (black solid line, secondary axis) and gaseous emissions curves (CO, green large hyphened line, CO_2, red dotted line, total hydrocarbons (HC), blue hyphened line, primary axis) for Tissue a) and Surgical b) masks.

The gaseous and conversion rate peaks of the Tissue mask occur at quite the same temperature (approximately 343.6 and 344.4 °C for the gaseous emissions, and 332.8 °C for the conversion rate), Fig. S4 a). The devolatilization peak of the conversion rate curve (first peak of the conversion rate curve) is higher and thinner than the gaseous peaks. The combustion peak (second peak) occurs at a temperature slightly higher than that of the CO and CO_2 emissions (454.5 °C against 452.2 and 448.7 °C). It is much lower than the second gaseous peaks.
For the Surgical mask, the peak of the conversion rate curve occurs at a much lower temperature than the gaseous peaks: 271.2 against 376.2, 376.6 and 377.7 °C, Fig. S4 b).